

Nuclear charge radius of ^8He

P. Mueller,^{1,*} I. A. Sulai,^{1,2} A. C. C. Villari,³ J. A. Alcántara-Núñez,³
 R. Alves-Condé,³ K. Bailey,¹ G. W. F. Drake,⁴ M. Dubois,³ C. Eléon,³ G.
 Gaubert,³ R. J. Holt,¹ R. V. F. Janssens,¹ N. Lécèsne,³ Z.-T. Lu,^{1,2} T.
 P. O'Connor,¹ M.-G. Saint-Laurent,³ J.-C. Thomas,³ and L.-B. Wang⁵

¹*Physics Division, Argonne National Laboratory, Argonne, Illinois 60439, USA*

²*Department of Physics and Enrico Fermi Institute,
 University of Chicago, Chicago, Illinois 60637, USA*

³*GANIL (IN2P3/CNRS-DSM/CEA),*

B.P. 55027 F-14076 Caen Cedex 5, France

⁴*Physics Department, University of Windsor,
 Windsor, Ontario, Canada N9B 3P4*

⁵*Los Alamos National Laboratory, Los Alamos, New Mexico 87545, USA*

(Dated: October 26, 2018)

Abstract

The root-mean-square (rms) nuclear charge radius of ^8He , the most neutron-rich of all particle-stable nuclei, has been determined for the first time to be 1.93(3) fm. In addition, the rms charge radius of ^6He was measured to be 2.068(11) fm, in excellent agreement with a previous result. The significant reduction in charge radius from ^6He to ^8He is an indication of the change in the correlations of the excess neutrons and is consistent with the ^8He neutron halo structure. The experiment was based on laser spectroscopy of individual helium atoms cooled and confined in a magneto-optical trap. Charge radii were extracted from the measured isotope shifts with the help of precision atomic theory calculations.

*Electronic address: pmueller@anl.gov

Precision measurements of nuclear structure in light isotopes are essential for a better understanding of nuclei and of the underlying interactions between protons and neutrons. *Ab initio* calculations of light nuclei provide quantitative predictions of nuclear properties based on empirical nucleon-nucleon and three-nucleon interactions [1, 2]. Investigations of very neutron-rich isotopes, among which the lightest are ${}^6\text{He}$ ($t_{1/2} = 807$ ms) and ${}^8\text{He}$ ($t_{1/2} = 119$ ms), present especially stringent tests for these calculations as they probe aspects of the interactions that are less prevalent in nuclei closer to stability.

The differences in charge radii in the helium isotopes, where the two protons are predominantly in a relative s-state, reflect primarily the center-of-mass motion of the protons with respect to the neutrons. Therefore, the charge radius is especially sensitive to neutron correlations. The two excess neutrons in ${}^6\text{He}$ and the four in ${}^8\text{He}$ form a halo with respect to a ${}^4\text{He}$ core (or α -particle) [3]. The excess neutron pair in ${}^6\text{He}$ is correlated in such a way that the recoil motion of the core results in an increased charge radius [4]. In ${}^8\text{He}$, the four excess neutrons are expected to be correlated in a more spherically symmetric way and this recoil effect is expected to be smaller.

Here, we report on the first measurements of the nuclear charge radius of ${}^8\text{He}$. Neutral helium atoms were laser cooled and confined in a magneto-optical trap, and the isotope shift $\delta\nu_{A,A'}$ of an atomic transition between isotopes A and A' was determined by laser spectroscopy. This isotope shift can be expressed as:

$$\delta\nu_{A,A'} = \delta\nu_{A,A'}^{\text{MS}} + K_{\text{FS}} \delta\langle r^2 \rangle_{A,A'}. \quad (1)$$

The mass shift $\delta\nu_{A,A'}^{\text{MS}}$ and the field shift constant K_{FS} of this two-electron system have both been precisely calculated [5], so that the change in mean-square nuclear charge radii $\delta\langle r^2 \rangle_{A,A'}$ between the two isotopes can be extracted from the measured isotope shift. Combined with a previous measurement on ${}^6\text{He}$ [4] and earlier studies of the two stable isotopes, ${}^3\text{He}$ [6] and ${}^4\text{He}$ [7], there is now a complete picture of the evolution of nuclear charge radii in the helium isotopic chain.

The experiment was carried out at the GANIL facility where ${}^6\text{He}$ and ${}^8\text{He}$ were simultaneously produced from a primary beam of 75 MeV/u ${}^{13}\text{C}$ impinging on a heated (~ 2000 K) graphite target. Low-energy (20 keV) beams of either ${}^6\text{He}$ or ${}^8\text{He}$ with yields of around 1×10^8 and 5×10^5 ions per second, respectively [8], were delivered to an adjacent low-radiation area where the helium ion beam was stopped in a hot, 1 cm² sized graphite foil for

neutralization. The released neutral, thermal helium atoms were pumped within 250 ms into the atomic beam apparatus resulting in rates of approximately $5 \times 10^7 \text{ s}^{-1}$ and $1 \times 10^5 \text{ s}^{-1}$ for ^6He and ^8He , respectively.

The trapping and spectroscopy setup has been previously described in detail in connection with the nuclear charge radius measurement of ^6He at Argonne’s ATLAS facility [4, 9]. The selective cooling and trapping of helium atoms in a magneto-optical trap (MOT) was pivotal for this work, providing single atom sensitivity, large signal-to noise ratios and high spectroscopic resolution. A beam of metastable helium atoms was produced through a LN_2 -cooled gas discharge. Transverse cooling and Zeeman slowing were applied to load the metastable helium atoms of a selected isotope into the MOT. Cooling and trapping were based on the cycling $2^3S_1 \rightarrow 2^3P_2$ transition at a wavelength of 1083 nm. The laser frequency for this transition was controlled to an accuracy of 100 kHz to allow reproducible switching between the respective isotopes. Detection and spectroscopy of the atoms captured in the MOT were performed by exciting one of the three cycling $2^3S_1 \rightarrow 3^3P_J$ transitions at 389 nm and imaging the fluorescence light onto a photomultiplier tube. The frequency of this probing laser was continuously measured relative to an iodine locked reference laser. The capture and detection efficiency of the setup were substantially improved compared to the previous ^6He measurement [4, 9] by optimizing many components throughout the apparatus. The signal-to-noise ratio of a single trapped atom reached 10 within 50 ms of integration time. The total capture efficiency was 1×10^{-7} and yielded capture rates of around 20,000 ^6He and 30 ^8He atoms per hour.

In the *capture* mode, the probing laser at 389 nm was tuned on resonance for maximum fluorescence and the trapping laser detuning and intensity were selected for highest capture efficiency. Single atom detection of ^8He triggered the system to switch into the *spectroscopy* mode for 200 ms, while for ^4He and ^6He the system was continuously switched to the *spectroscopy* mode with a rate of 2.5 Hz. During the *spectroscopy* mode, the fluorescence rate was recorded as a function of probing laser frequency by scanning the probing laser with a 83 kHz repetition rate over ± 9 MHz relative to the respective resonance center. Additionally, the detuning and intensity of the trapping laser were reduced, the slowing light was turned off, and the probing and trapping laser beams were alternately switched on and off with a 100 kHz repetition rate and a cycle of 2 μs probing vs. 8 μs trapping. This scheme was developed to eliminate AC Stark shifts caused by the trapping light while

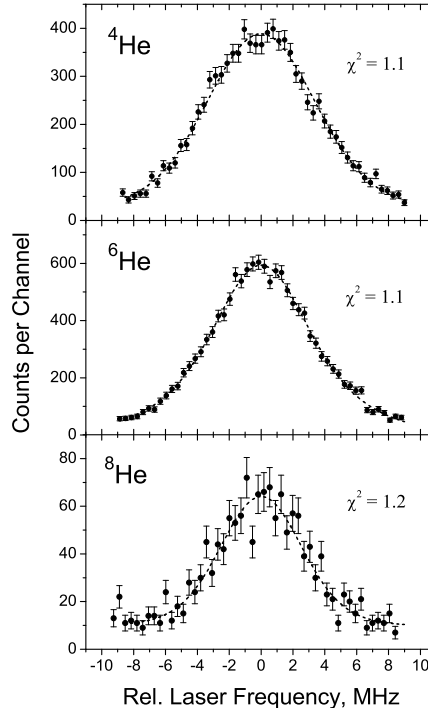


FIG. 1: Sample spectra for ${}^4\text{He}$, ${}^6\text{He}$ and ${}^8\text{He}$ taken on the $2^3S_1 \rightarrow 3^3P_2$ transition at a probing laser intensity of $\sim 3 \times I_{\text{sat}}$. Error bars are statistical uncertainties, the dashed lines represent least squares fits (with the listed reduced χ^2) using Voigt profiles. The apparent peak broadening towards lower masses is due to the $m^{-1/2}$ scaling of the residual Doppler width.

minimizing systematic heating and cooling of the atoms caused by the probing light.

A total of twelve sets of measurements for the ${}^6\text{He}$ - ${}^4\text{He}$ isotope shift and eight for ${}^8\text{He}$ - ${}^4\text{He}$ were taken during three days. The measurements for ${}^6\text{He}$ and the reference isotope ${}^4\text{He}$ were each performed at several settings for the probing laser intensity: from $\sim 3 \times I_{\text{sat}}$ down to $\sim 0.3 \times I_{\text{sat}}$, where $I_{\text{sat}} = 3.4 \text{ mW/cm}^2$ is the saturation intensity of the transition. Small systematic shifts of the resonance frequencies observed at high intensities showed no significant difference between ${}^4\text{He}$ and ${}^6\text{He}$, but were found to vary slightly over time, consistent with variations of the probing laser beam alignment. This effect was taken into account for the ${}^8\text{He}$ data, which could only be recorded with signal-to-noise ratios sufficient for single-atom detection, i.e., at $\sim 3 \times I_{\text{sat}}$.

Samples of resonance profiles for each isotope taken at $\sim 3 \times I_{\text{sat}}$ are given in Fig. 1. The ${}^8\text{He}$ peak represents data integrated over 60 individually trapped atoms accumulated in two hours, while the ${}^4\text{He}$ and ${}^6\text{He}$ peaks were typically acquired in less than one minute. All

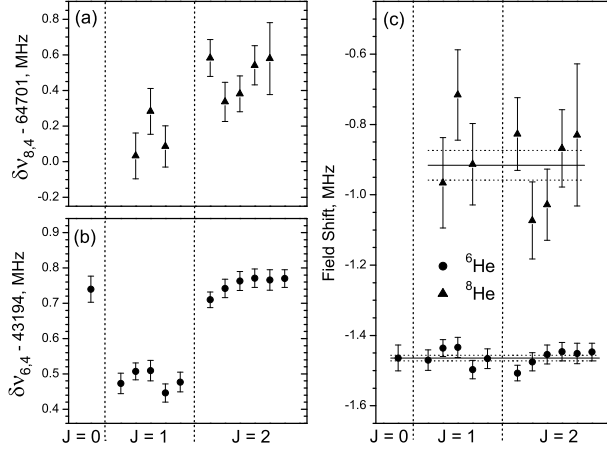


FIG. 2: Experimental isotope shifts relative to ^4He from the individual measurements for ^8He (a) and ^6He (b). As expected, the isotope shift depends on the J of the upper 3^3P_J state. However, the extracted field shift values plotted in (c) show no systematic J dependence for either isotope. The horizontal lines in (c) mark the weighted averages and statistical error bands of the field shift.

TABLE I: Weighted averages of the experimental isotope shifts $\delta\nu_{A,4}$ (including recoil correction) for the different transitions in ^6He and ^8He . The field shift $\delta\nu_{A,4}^{\text{FS}} = K_{\text{FS}} \delta\langle r^2 \rangle_{A,4}$ was calculated for each transition using the listed *theoretical* mass shift values $\delta\nu_{A,4}^{\text{MS}}$. All values are in MHz. The errors given in parentheses for $\delta\nu_{A,4}$ and $\delta\nu_{A,4}^{\text{FS}}$ include only statistical uncertainties.

Transition	$\delta\nu_{A,4}$	$\delta\nu_{A,4}^{\text{MS}}$	$\delta\nu_{A,4}^{\text{FS}}$
$^6\text{He } 2^3S_1 \rightarrow 3^3P_0$	43194.740(37)	43196.204	-1.464(37)
$2^3S_1 \rightarrow 3^3P_1$	43194.483(12)	43195.943	-1.460(12)
$2^3S_1 \rightarrow 3^3P_2$	43194.751(10)	43196.217	-1.466(10)
$^8\text{He } 2^3S_1 \rightarrow 3^3P_1$	64701.129(73)	64701.999	-0.870(73)
$2^3S_1 \rightarrow 3^3P_2$	64701.466(52)	64702.409	-0.943(52)

peaks could be fit well with Voigt profiles. The Gaussian widths of the fitted Voigt profiles scale with $m^{-1/2}$, as expected from a mass-independent temperature of the trapped atoms, and become smaller at lower intensity of the probing laser.

The isotope shifts for ^6He and ^8He relative to ^4He obtained in the individual measurements are plotted in Fig. 2 along with the extracted field shifts. Table I lists the weighted averages of isotope shifts and field shifts separately for the different fine structure levels 3P_J . The

isotope shift for the $2^3S_1 \rightarrow 3^3P_2$ transition in ^6He agrees with the previously published value of 43194.772(33) MHz [4] within the quoted *statistical* uncertainties. The isotope shift values for the different transitions in ^6He show variations by 250 kHz, as predicted by the atomic theory calculations. The extracted field shifts for all three transitions agree well within statistical uncertainties. This is a valuable consistency test for atomic theory as well as a check for a class of systematic errors in the experiment, since the strengths of these three transitions vary by a factor of up to five. Hence, the field shifts over all three transitions in ^6He were averaged as independent measurements, and likewise for the two transitions observed in ^8He .

The final field shift results for both isotopes are listed in Table II along with the contributions from statistical and systematic uncertainties. Besides photon counting statistics, there are two additional random effects: the frequency drift of the reference laser and variations in the power-dependent frequency shift due to small drifts in the probing laser alignment. Both lead to significant scattering of the results during the roughly two hour integration time needed for each ^8He measurement, but are insignificant in the case of ^6He . A significant systematic uncertainty is caused by Zeeman shifts that might have varied among isotopes if the atoms were not located exactly at the zero B-field position of the MOT. Limits on this effect are set conservatively at ≤ 30 kHz for the ^6He - ^4He isotope shift, and ≤ 45 kHz for ^8He - ^4He . Moreover, two corrections are applied to the measured isotope shifts as listed in Table II: photon recoil and nuclear polarization. The first was trivially and accurately calculated. The latter depends on the nuclear polarizability, which was extracted from measurements of the electric dipole strength [10, 11]. The uncertainty in the nuclear mass enters as an additional systematic effect via the theoretical mass shift. This effect is the single biggest contribution to the final uncertainty for ^8He , but plays only a minor role for ^6He . Improved mass measurements for both isotopes are in preparation, using Penning trap mass spectrometry [12].

Table III lists the final results for the difference in mean-square charge radius of ^6He and ^8He relative to ^4He , which follow directly from the field shift using $K_{\text{FS}} = 1.008 \text{ fm}^2/\text{MHz}$ from atomic theory [5]. The absolute charge radii for both isotopes are based on a value of 1.676(8) fm for the ^4He charge radius [7]. For a comparison of our results on rms charge radii $\langle r^2 \rangle_{\text{ch}}^{1/2}$ to the rms *point-proton* radii $\langle r^2 \rangle_{\text{pp}}^{1/2}$, typically quoted by theoretical papers, the relation $\langle r^2 \rangle_{\text{pp}} = \langle r^2 \rangle_{\text{ch}} - \langle R_{\text{p}}^2 \rangle - \frac{3}{4M_{\text{p}}^2} - \frac{N}{Z} \langle R_{\text{n}}^2 \rangle$ was used, which takes into account contributions

TABLE II: Statistical and systematic uncertainties and corrections on the combined results for the field shifts of ${}^6\text{He}$ and ${}^8\text{He}$ relative to ${}^4\text{He}$. All values are in MHz.

	${}^6\text{He}$		${}^8\text{He}$	
	value	error	value	error
<i>Statistical</i>				
Photon counting		0.008		0.032
Probing laser alignment		0.002		0.012
Reference laser drift		0.002		0.024
<i>Systematic</i>				
Probing power shift				0.015
Zeeman shift		0.030		0.045
Nuclear mass		0.015		0.074
<i>Corrections</i>				
Recoil effect	0.110	0.000	0.165	0.000
Nuclear polarization	-0.014	0.003	-0.002	0.001
$\delta\nu_{A,4}^{\text{FS}}$ combined	-1.478	0.035	-0.918	0.097

TABLE III: Relative and absolute charge radii for all particle-stable helium isotopes. The absolute ${}^3\text{He}$ radius is calculated with the relative value from Ref. [6] and the absolute ${}^4\text{He}$ value from Ref. [7]. Values for ${}^6\text{He}$ and ${}^8\text{He}$ are from this work.

	${}^3\text{He}$	${}^4\text{He}$	${}^6\text{He}$	${}^8\text{He}$
$\delta\langle r^2 \rangle_{A,4}$, fm ²	1.059(3)	-	1.466(34)	0.911(95)
$\langle r^2 \rangle_{\text{ch}}^{1/2}$, fm	1.967(7)	1.676(8)	2.068(11)	1.929(26)

from the mean-square charge radii of the proton and neutron (with $\langle R_p^2 \rangle = 0.769(12)$ fm² and $\langle R_n^2 \rangle = -0.1161(22)$ fm² [13]) and the Darwin-Foldy term $\frac{3}{4M_p^2} = 0.033$ fm² [14]. The effects of nuclear spin-orbit interaction and meson exchange currents, expected to be on the order of or below the experimental uncertainties, are not taken into account and will require further theoretical investigation.

The experimental rms point-proton radii from this work are plotted in Fig. 3 along with matter radii (i.e., point-nucleon radii) extracted from strong interaction cross section

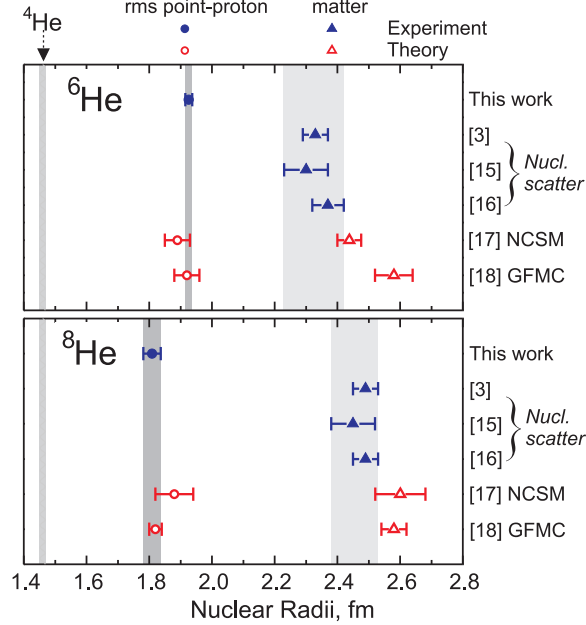


FIG. 3: Comparison of rms point-proton radii (circles) and matter radii (triangles) for ${}^6\text{He}$ and ${}^8\text{He}$ between experiment (solid symbols) and theory (open symbols). The vertical bands represent *experimental* error bands, consistent with the spread and error bars of the reported values, and the ${}^4\text{He}$ rms point-proton radius from [7]. For comparison, the ${}^3\text{He}$ point-proton radius is 1.77(1) fm [6].

measurements [3, 15, 16]. While the latter are model dependent, different methods give consistent matter radii. The matter radius for ${}^4\text{He}$ should be the same as the indicated point-proton radius. Also given in Fig. 3 are the values from *ab initio* calculations based on the no-core shell model (NCSM) [17] and Green’s function Monte Carlo (GFMC) techniques [18]. Apart from those, there are a number of cluster model calculations providing values for rms point-proton and matter radii of both isotopes [19].

Most strikingly, the rms charge radius *decreases* significantly from ${}^6\text{He}$ to ${}^8\text{He}$, while the matter radius seems to *increase*. The larger matter radius of ${}^8\text{He}$ is consistent with there being more neutrons and more nucleons altogether. On the other hand, the larger charge radius of ${}^6\text{He}$ is consistent with the interpretation that the two neutrons are correlated so that on average they spend more time together on one side of the core rather than on opposite sides. As a result, the recoil motion of the α -like core against the correlated pair of neutrons smears out the charge distribution. In ${}^8\text{He}$, the four excess neutrons are distributed in a more spherically symmetric fashion in the halo and the smearing of the

charge in the core is correspondingly less, leading to a *reduction* in the charge radius. These effects are reproduced rather well by *ab initio* calculations, giving further confidence in our understanding of nuclear forces and in the method of calculation.

Acknowledgments

We acknowledge the contribution of the GANIL accelerator (Service des Accélérateurs) and physical technical (Service Techniques de la Physique) staff. We thank J. P. Schiffer, S. Pieper and R. Wiringa for stimulating discussions, and J. P. Greene, D. Henderson, S. M. Hu, C. L. Jiang, M. Notani, R. C. Pardo, K. E. Rehm, B. Shumard and X. Tang for contributions in the early phase of this experiment. This work was supported by the U.S. Department of Energy, Office of Nuclear Physics, under Contract No. DE-AC02-06CH11357. G. Drake acknowledges support by NSERC and by SHARCnet. Experiment performed at GANIL (IN2P3/CNRS - DSM/CEA).

-
- [1] S. C. Pieper, V. R. Pandharipande, R. B. Wiringa and J. Carlson, Phys. Rev. C **64**, 014001 (2001).
 - [2] P. Navrátil, J. P. Vary, and B. R. Barrett, Phys. Rev. C **62**, 054311 (2000).
 - [3] I. Tanihata *et al.*, Phys. Lett. B **289**, 261 (1992).
 - [4] L.-B. Wang *et al.*, Phys. Rev. Lett. **93**, 142501 (2004).
 - [5] G. W. F. Drake, Nucl. Phys. A **737**, 25 (2004).
 - [6] D. Shiner, R. Dixson and V. Vedantham, Phys. Rev. Lett. **74**, 3553 (1995); D. C. Morton, Q. Wu and G. W. F. Drake, Phys. Rev. A **73**, 034502 (2006).
 - [7] I. Sick, Phys. Lett. B **116**, 212 (1982).
 - [8] F. Landré-Pélémoine *et al.*, Nucl. Phys. A **701**, 491c (2002).
 - [9] L.-B. Wang, PhD Thesis, University of Illinois at Urbana-Champaign, 2004.
 - [10] K. Pachucki and A. M. Moro, Phys. Rev. A **75**, 032521 (2007).
 - [11] Y. Iwata *et al.*, Phys. Rev. C **62**, 064311 (2000).
 - [12] K. Blaum *et al.*, ISOLDE Proposal CERN-INTC-2002-021/INTC-P-160 (2002); K. Blaum, *priv. comm.* (2007); J. Dilling, *priv. comm.* (2007).

- [13] W.-M. Yao *et al.* (Particle Data Group), *J. Phys. G* **33**, 1 (2006).
- [14] J. L. Friar, J. Martorell, and D. W. L. Sprung, *Phys. Rev. A* **56**, 4579 (1997).
- [15] G. D. Alkhazov *et al.*, *Phys. Rev. Lett.* **78**, 2313 (1997).
- [16] O. A. Kiselev *et al.*, *Europ. Phys. J. A* **25** Suppl. 1, 215 (2005).
- [17] E. Caurier and P. Navrátil, *Phys. Rev. C* **73**, 021302(R) (2006).
- [18] S. C. Pieper, Argonne National Laboratory, unpublished information (2007); arXiv:0711.1500 [nucl-th].
- [19] J. Wurzer and H. M. Hofmann, *Phys. Rev. C* **55**, 688 (1997); K. Varga, Y. Suzuki and Y. Ohbayasi, *Phys. Rev. C* **50**, 189 (1994); V. S. Vasilevsky *et al.*, *Phys. Atom. Nucl.* **60**, 343 (1997); A. V. Nesterov, V. S. Vasilevsky and O. F. Chernov, *Phys. Atom. Nucl.* **64**, 1409 (2001); T. Neff and H. Feldmeier, *Nucl. Phys. A* **738**, 357 (2004); Y. Kanada-En'yo, *Phys. Rev. C* **76**, 044323 (2007).